Analysis and Suppression of Zero Sequence Circulating Current in Open Winding PMSM Drives with Common DC Bus

Hanlin Zhan, Z.Q. Zhu, *Fellow*, *IEEE* and M. Odavic
Department of Electronic and Electrical Engineering
The University of Sheffield, Mappin Street, Sheffield S1 3JD, UK
hzhan2@sheffield.ac.uk, z.q.zhu@sheffield.ac.uk and m.odavic@sheffield.ac.uk

***Abstract* – In this paper, the zero sequence circulating current in open winding (OW) permanent magnet synchronous machine (OW-PMSM) drives with common DC bus is systematically analysed for the first time. It is revealed that the zero sequence circulating current is affected by zero sequence back electromotive force (EMF), cross coupling voltages in zero sequence, from the machine side, pulse width modulation (PWM) induced zero sequence voltage and inverter nonlinearity, from the inverter side. Particularly, the influences from the cross coupling voltages in zero sequence and parasitic effect of inverter nonlinearity are investigated for the first time in this paper. Then the synthetic model of the equivalent zero sequence circuit is proposed as well. Each cause is studied independently via analytical modelling, finite element analysis and experiments. Meanwhile, to tackle this issue, the relevant suppression strategy using frequency adaptive proportional resonant controller is presented and tested on the 3kW OW-PMSM platform.**

***Keywords*—Circulating current, inverter nonlinearity, open winding, PMSM, zero sequence.**

I. Introduction

Open winding (OW) machine drives are recently investigated and developed for electrical vehicle (EV) propulsion, wind power generation and industrial motor drives [1]-[4] owing to high DC bus utilization and potential fault tolerant capability. Meanwhile, the permanent magnet synchronous machines (PMSMs) are also widely used in various industrial applications due to high efficiency, torque density and power factor [5] [6]. Specifically, the OW-PMSM inheriting the synthesis of OW topology and PMSM is attracting more and more research attentions [1]-[4] [7].

In general, the OW drive topologies can be divided into two types, viz., OW drive with common DC bus and isolated DC bus. The common DC bus one essentially requiring no isolation transformer can reduce the system volume, weight and cost. But the zero sequence path existing in the OW drive with common DC bus enables additional zero sequence current to circulate within the system including the OW drive and machine. The zero sequence circulating current will consequently cause unwanted power losses, torque ripple and system instability [4] [7]. Hence, it is necessary to investigate the origins of the zero sequence circulating current and seek solution to suppress it.

At present, zero sequence back EMF is regarded as the major disturbance source of OW-PMSM drives in the majority of the relevant research papers [4] [7] [8] [14]. Meanwhile, zero sequence circulating current due to inverter nonlinearity [9] and PWM modulated voltage [10] are also investigated independently, which could also be applied to OW-induction machine (IM) (OW-IM). However, according to current research, the possible origins of the circulating current are not fully identified in literature. Meanwhile, the accurate mathematical model and thorough mechanism explanation are not presented as well. In [11], a simple sinusoidal feedforward strategy is adopted to suppress the zero sequence circulating current. This strategy might not be able to tolerate the variation of operating condition. In [7], a zero vector redistribution method is proposed to control the zero sequence current and only the zero sequence back EMF is regarded as the major disturbance source. As for OW-IM, the authors in [9] investigate the influence of inverter nonlinearity that could also cause zero sequence circulating current. However, due to the parasitic effects of the switching device, it is not revealed in literature that the inverter nonlinearities will no longer induce zero sequence circulating current within small current range, as will be presented in this paper. Meanwhile, the PWM strategy modulated zero sequence voltage is studied in [10] and the phase shift based method is proposed for the cancellation. Besides, in [12], the authors propose an OW topology with 4 additional auxiliary bidirectional switches enabling a switched neutral point structure to suppress the third harmonic currents and reach a higher DC bus utilization. A PI controller is used in [8] to suppress the zero sequence circulating current. The static error of PI controller for alternating signal still exists. With regard to five-phase OW drives, an SVPWM scheme with common mode voltage elimination ability for single DC supply is proposed and two of the possible switching sequences are chosen for further investigation [13]. Moreover, in [14], a zero sequence current estimator auxiliary vector control method to compensate zero sequence EMF is proposed based on sinusoidal PWM strategy.

In this paper, the integrated formation mechanism, mathematical model and suppression strategy for zero sequence circulating current are studied. The main contribution is proposing thorough mathematical model of equivalent zero sequence circuit by including the influences of zero sequence back EMF, cross coupling voltages in zero sequence, inverter nonlinearity and PWM modulated zero sequence voltage. Of which, the influence of zero sequence voltages due to the parasitic effects of switching devices and the cross coupling voltages in zero sequence are also investigated for the first time in this paper. Finally, the proposed suppression effectively

978-1-5090-0737-0/16/$31.00

eliminate the alternating zero sequence, which is validated experimentally. This paper is organized as follows: In Section II and III, the zero sequence disturbances from machine and inverter side are investigated, respectively. In Section IV, the synthetic disturbance model is summarized. The suppression strategy using frequency adaptive proportional resonant (FA-PR) controller is presented in Section V. The experimental validation is presented in Section VI.

II. Zero Sequence Disturbances From Machine Side

A. Zero Sequence Back EMF

Third harmonic back EMF is usually observed in the phase back EMF of PMSM except for those with specific winding configurations or structure designs. Due to zero angle shift between phases, third harmonic back EMF in the phase demonstrates as zero sequence back EMF. The magnetization type, magnet shaping and teeth saturation can all impose influence on the third harmonic flux density distribution inducing zero sequence back EMF. The winding factor of the third harmonic exhibits damping effect for the third harmonic back EMF in the phase. Although third harmonic back EMF has no influence on the conventional Y-connected single three phase machine system, it behaves as a voltage source in the equivalent zero sequence circuit of the OW-PMSM. Fig. 1 shows the phase back EMF waveform and the spectrum analysis of a 3kW OW-PMSM with 96/slot-32/pole combination at 10rpm. The specification of this prototype machine can be found in Appendix A. It can be seen that the third harmonic component is dominant in the phase back EMF.

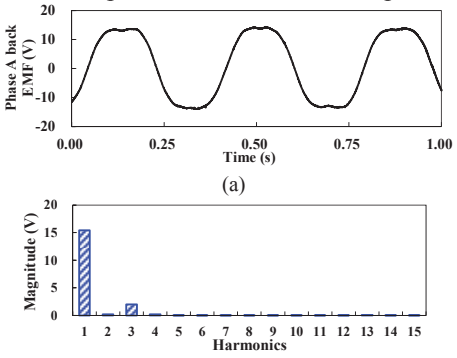

Fig. 1 Measured phase back EMF waveform and spectrum analysis of the 96/slot-32/pole OW-PMSM. (a) Waveform. (b) Spectrum.

B. Cross Coupling Voltages in Zero Sequence

Zero sequence signals are usually decoupled from *dq*-axis under the assumption of ideal synchronous machine. In the assumption, the amplitudes of the second harmonics of the phase self-inductance L_{S2} and the mutual-inductance M_{S2} should satisfy $L_{S2}= M_{S2}$ which is also called as the condition of ideal synchronous machine. Both L_{S2} and M_{S2} contribute to the saliency of the synchronous machine. However, this condition is not always satisfied when different winding configurations of the PMSMs are applied. Meanwhile, this discrepancy consequently leads to the coupling between zero sequence and *dq* axes. The coupling inductance component can be defined as $L_{\Delta}=(L_{S2}-M_{S2})/2$. Typically, Fig. 2 shows the phase self- and mutual-inductances of the 12/slot-10/pole OW-PMSM with double layer concentrated winding and the 96/slot-32/pole OW-PMSM with single layer winding distribution by using 2 dimensional (2D) finite element (FE). The specification of the 12/slot-10/pole OW-PMSM prototype machine can be found in Appendix A. The inductances are calculated according to the method proposed in [15]. It can be seen that the coupling inductance of the 12/slot-10/pole OW-PMSM is much more obvious than that of the 96/slot-32/pole OW-PMSM.

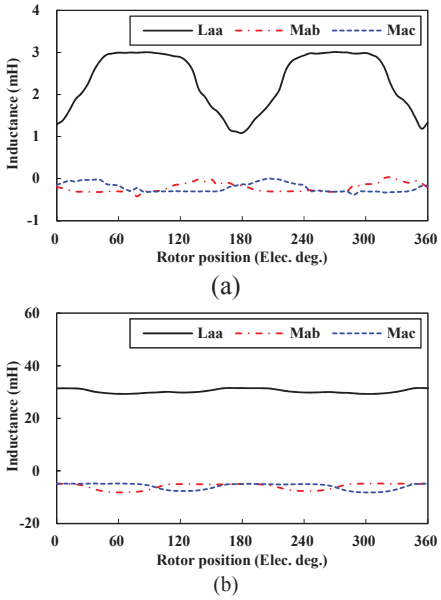

Fig. 2 Phase self- and mutual-inductances curves of the OW-PMSMs calculated by 2D-FE. (a) 12/slot-10/pole OW-PMSM with double layer concentrated winding. (b) 96/slot-32/pole OW-PMSM with single layer overlapping winding.

Meanwhile, the difference of the coupling inductance of the two OW-PMSMs can be understood via the phase A armature winding current flux-linkage distributions those are shown in Fig. 3. In Fig. 3 (a), only phase A is excited by 5A current component and the majority of the flux-linkage is self-closed. A small quantity of flux-linkage is closed via phase B, which represents the mutual inductance characteristic. In Fig. 3 (b), more flux-linkage generated by phase A is closed via phase B due to the overlapping coils. The winding distribution affects the coupling inductance of the OW-PMSM. The overlapping winding distribution usually leads to a smaller coupling inductance characteristic for the OW-PMSM.

If the condition of $L_{S2}=M_{S2}$ is not satisfied, the inductance matrix transformed into *dq*0 coordinate has cross coupling terms between *dq* axes and zero sequence, namely, L_{Δ}. Hence, the *d*- and *q*-axis currents will consequently impose coupled voltage components into zero sequence and induce corresponding zero sequence circulating current. Therefore, it is necessary to take the influence of these cross coupling components in zero sequence into consideration for a comprehensive circulating current modelling. When $L_{S2}\neq M_{S2}$, the coupled inductance terms between zero sequence and *dq* axes can be expressed as

$$L_{d0} = \frac{L_{0d}}{2} = L_{\Delta}\cos 3\theta \tag{1}$$

$$L_{q0} = \frac{L_{0q}}{2} = -L_{\Delta}\sin 3\theta \tag{2}$$

where $\omega t=\theta$.

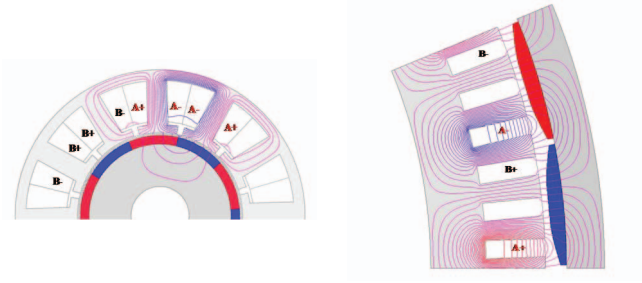

(a) (b)

Fig. 3 Phase A armature winding current flux-linkage distribution of the OW-PMSMs. (a) 12/slot-10/pole OW-PMSM. (b) 96/slot-32/pole OW-PMSM.

Hence, the corresponding induced voltages due to *dq*-axis currents imposed on zero sequence are

$$u_{0-id} = \frac{d\psi_{d0}}{dt} = \frac{d(i_d L_{d0})}{dt} = -3\omega i_d L_{\Delta}\sin 3\omega t \tag{3}$$

$$u_{0-iq} = \frac{d\psi_{q0}}{dt} = \frac{d(i_q L_{q0})}{dt} = -3\omega i_q L_{\Delta}\cos 3\omega t\,. \tag{4}$$

The complete derivation is presented in Appendix B. Meanwhile, it can be seen that these voltage disturbances can be regarded as current controlled voltage sources (CSVSs) based on *dq*-axis currents.

Fig. 4 shows the 2D-FE results of the zero sequence induced voltages of a 12/slot-10/pole fractional OW-PMSM with non-overlapping winding configuration (L_{Δ}>0) with and without 4A *q*-axis current. It can be seen that the zero sequence induced voltage is shifted and distorted at on-load condition due to the cross coupling voltage components from *dq* axes. Fig. 5 shows the 2D FE results of the zero sequence induced voltages of a 96/slot-32/pole OW-PMSM with overlapping winding configuration ($L_{\Delta}\approx$0) with and without 5A *q*-axis current. It can be found that *q*-axis current imposes much less influence on the zero sequence induced voltage of the overlapping winding OW-PMSM.

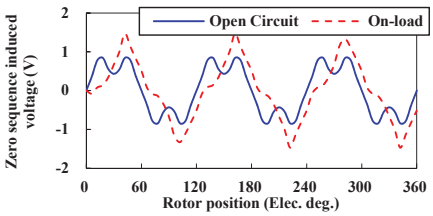

Fig. 4 Zero sequence induced voltage of the 12/slot-10/pole OW-PMSM at open circuit and on-load conditions.

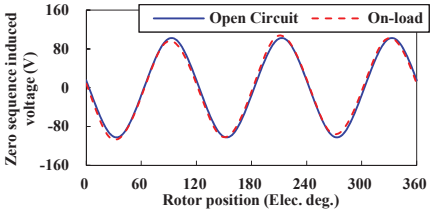

Fig. 5 Zero sequence induced voltage of the 96/slot-32/pole OW-PMSM at open circuit and on-load conditions.

III. Zero Sequence Disturbance From Inverter Side

A. Equivalent Zero Sequence Modulation Voltage

In conventional space vector pulse width modulation (SVPWM) strategy, the equivalent zero sequence modulation signal is quasi-triangle wave, which induces no zero sequence current due to the open circuit characteristic of the equivalent zero sequence circuit. However, for the OW-PMSM with common DC bus, the existence of zero sequence circuit enables the equivalent zero sequence modulated voltage to induce corresponding circulating current. Hence, the phase shift based SVPWM [10] is used to eliminate the relevant part of zero sequence disturbance voltage. The PWM strategy induced zero sequence disturbance voltage can be effectively eliminated via phase shift based SVPWM. However, the other zero sequence disturbance voltage sources are not eliminated effectively. Figs. 6 and 7 show the synthetic and separate modulation signals for each inverter with 120º and 180º shift when 40Hz and 0.5 p.u. reference is given. The 120º shift method shows no modulated zero sequence voltage as expected. Meanwhile, the 180 shift method shows typical quasi-triangle waveform in zero sequence.

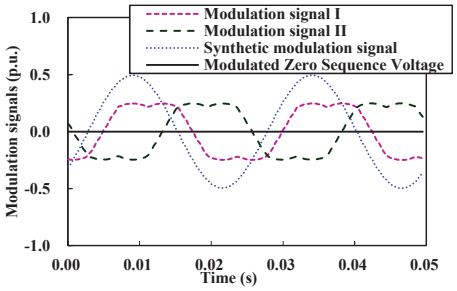

Fig. 6 Synthetic and separate modulation signals for each inverter with 120º shift (40Hz, 0.5 p.u.).

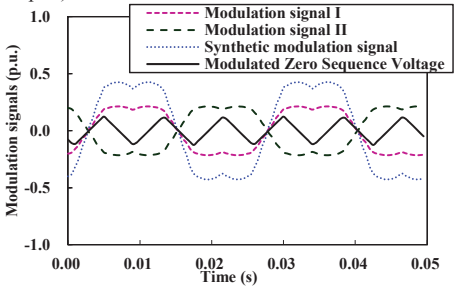

Fig. 7 Synthetic and separate modulation signals for each inverter with 180º shift (40Hz, 0.5 p.u.).

B. Inverter Nonlinearity

The inverter nonlinearity characteristic of the OW-PMSM drive with common DC bus is different from conventional single three phase machine drives since the inherently contained 3rd, 9th … components in phase distortion voltage induced by inverter nonlinearity can only float the neutral point voltage of the Y connected single three phase machine. Whereas, those zero sequence components due to inverter nonlinearity will be superimposed on the equivalent zero sequence modulation voltage discussed in Section II (A), as part of the zero sequence voltage disturbance from inverter side.

The inverter nonlinearity for OW drive is simply modelled via sign function in [9] and the equivalent zero sequence disturbance voltage is approximately regarded as alternating square wave, in which the third harmonic is dominant. However, the precise model of inverter nonlinearity requires the description for parasitic effects during small current range, namely, near to zero current [16] [17]. The inverter nonlinear distortion voltage at small current range exhibits resistive effect instead of saturation voltage drop since the parasitic capacitances. The influence of the corresponding effects on OW drives has not been reported yet. The modelling is established as follows.

Firstly, the phase distortion voltage error can be modelled as a nonlinear function [16] depending on phase current, viz.,

$$\Delta u_{err-x} = f(i_x) = 2\Delta U\left(\frac{1}{1+e^{-ki_x}} - \frac{1}{2}\right) \tag{5}$$

where $\Delta u_{err\text{-}x}$ represents arbitrary phase distortion voltage, i_x represents arbitrary phase current, k and ΔU are the distortion voltage model parameters describing the nonlinearity. Higher parasitic capacitance usually leads to lower k. The longer configured dead time and higher DC bus result in larger ΔU. The differential of (5) relative to phase current is usually defined as high frequency (HF) equivalent resistance [17]. Fig. 8 shows the phase voltage error and HF equivalent resistance curves for arbitrary phase.

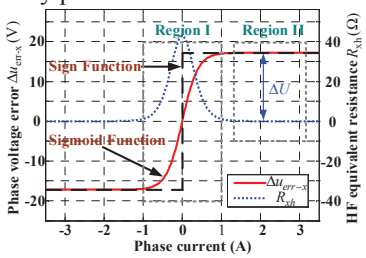

Fig. 8 Phase voltage error and HF equivalent resistance [17].

The sigmoid type function provides more detail information than the conventional sign function to describe the small current signal characteristics in region I, which is shown in Fig. 8. Within region I, the inverter nonlinearity demonstrates resistive characteristics due to the parasitic effects of the switching device, instead of saturation voltage distortion. Hence, the inverter nonlinearity represents equivalent three phase resistance network in series with the machine for small current signals and almost no zero sequence disturbance voltage will be introduced under this condition. However, the zero sequence disturbance voltage becomes dominant when the phase current escapes from the small current region I.

The synthetic distortion voltage is

$$\begin{bmatrix} u_{d-dt} \\ u_{q-dt} \\ u_{0-dt} \end{bmatrix} = \frac{2}{3}\begin{bmatrix} \cos\theta & \cos(\theta-\frac{2\pi}{3}) & \cos(\theta+\frac{2\pi}{3}) \\ -\sin\theta & -\sin(\theta-\frac{2\pi}{3}) & -\sin(\theta+\frac{2\pi}{3}) \\ \frac{1}{2} & \frac{1}{2} & \frac{1}{2} \end{bmatrix}\begin{bmatrix} f(i_a) \\ f(i_b) \\ f(i_c) \end{bmatrix} \tag{6}$$

Specifically, the zero sequence disturbance voltage is

$$u_{0-dt} = \frac{f(i_a)+f(i_b)+f(i_c)}{3} \tag{7}$$

Fig. 9 shows the zero sequence distortion voltage and three phase distortion voltages when the three phase current amplitudes are 3A and 0.25A. It can be seen that the zero sequence distortion voltage demonstrates as third quasi-square wave when the phase current is beyond region I and the zero sequence distortion voltage is not dominant when the phase current is within region I. The model will be validated via experiment in Section VI on three phase reactor load with phase shift SVPWM strategy to avoid influence from other zero sequence disturbance sources.

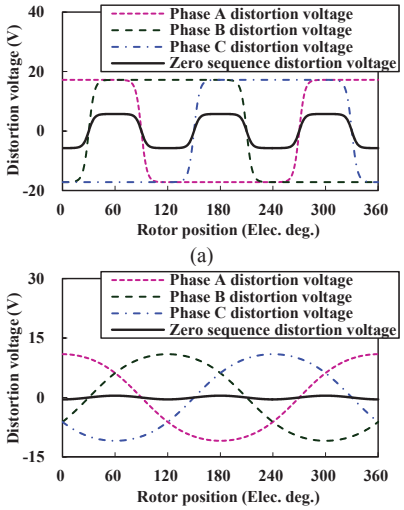

Fig. 9 Three phase and synthetic zero sequence distortion voltages beyond and within linear region. (a) Distortion voltages beyond linear region. (b) Distortion voltages within linear region.

IV. Synthetic Disturbance Model

According to the analysis in Section II and III, the zero sequence disturbance could contain 4 possible disturbance sources. The zero sequence back EMF and cross coupling voltages in zero sequence exist in the machine side. The equivalent zero sequence modulation voltage and inverter nonlinearity are from inverter side. Of which, the zero sequence disturbance voltages from inverter nonlinearity and cross coupling in zero sequence perform as CCVSs.

Fig. 10 shows the synthetic disturbance model, namely, the equivalent zero sequence circuit considering all possible disturbance voltage sources where $g(i_a,i_b,i_c)=[f(i_a)+f(i_b)+f(i_c)]/3$, $g_d(i_d)=-6\omega i_d L_\Delta \sin 3\omega t$ and $g_q(i_q)=6\omega i_q L_\Delta \cos 3\omega t$ describing the characteristics of the CCVSs. u_0 represents the modulated zero sequence voltage depending on the modulation strategy and whether it is steerable or not. e_0 is the zero sequence back EMF which is mainly the third harmonic component. Hence, the synthetic zero sequence differential equation can be expressed as

$$u_0 = u_{0-dt} + u_{0-id} + u_{0-iq} + e_0 + R_s i_0 + L_0 \frac{di_0}{dt}$$
$$= \frac{f(i_a) + f(i_b) + f(i_c)}{3} - 6\omega i_d L_\Delta \sin 3\omega t \quad (8)$$
$$+6\omega i_q L_\Delta \cos 3\omega t + 3\omega \psi_{f0} \sin 3\omega t + R_s i_0 + L_0 \frac{di_0}{dt}$$

where ψ_{f0} represents the zero sequence flux linkage.

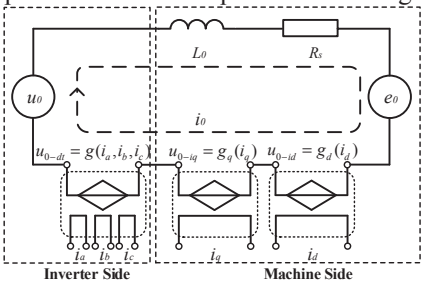

Fig. 10 Equivalent zero sequence circuit.

V. Suppression Strategy

On the basis of Section IV, it can be seen that only u_0 is steerable and the other 3 sources might vary within the whole operation range of the OW-PMSM. The alternating zero sequence circulating current is mainly induced by the third harmonic disturbance whose frequency, phase and amplitude are motor operation frequency and armature winding current dependent. Hence, the corresponding suppression strategy shown in Fig. 11 is proposed to attenuate the zero sequence circulating current.

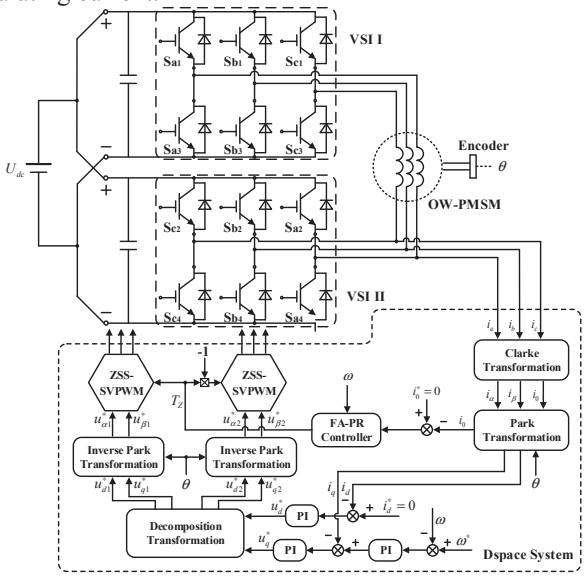

Fig. 11 Suppression strategy of the OW-PMSM for zero sequence circulating current attenuation using FA-PR controller.

Of which, the zero sequence steerable space vector pulse width modulation (ZSS-SVPWM) is developed to provide a controllable zero sequence component. The flow chart of the ZSS-SVPWM strategy is shown in Fig. 12. The zero sequence component is no longer essentially generated by the SVPWM but superimposed by the zero sequence controller output. Hence, the over modulation process should be redesigned by considering the influence from the additional zero sequence component, which is also shown in Fig. 12.

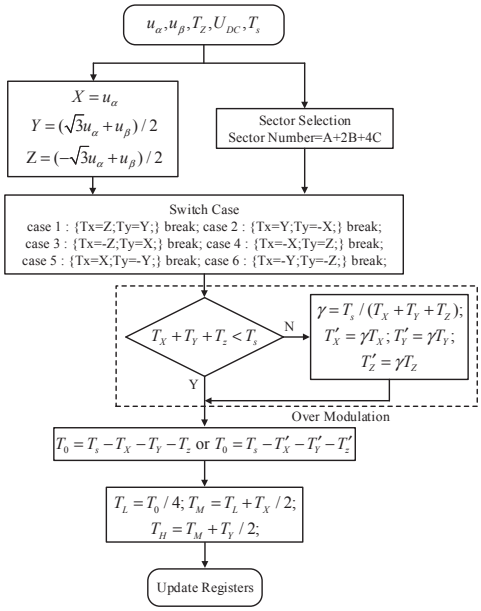

Fig. 12 Flow chart of the ZSS-SVPWM strategy.

In addition, the quasi-triangle wave generated by the SVPWM is also one the of the zero sequence disturbance sources, and therefore, the relevant disturbance burden will be imposed on the zero sequence controller. In order to reduce the controller burden, the phase shift based method is combined to eliminate the disturbance due to modulation strategy, which is achieved by decomposition transformation, viz.,

$$\begin{bmatrix} u_{d1} \\ u_{q1} \\ u_{d2} \\ u_{q2} \end{bmatrix} = \frac{1}{2} \cdot \begin{bmatrix} 1 & \tan(\pi/6) \\ -\tan(\pi/6) & 1 \\ -1 & \tan(\pi/6) \\ -\tan(\pi/6) & -1 \end{bmatrix} \cdot \begin{bmatrix} u_d \\ u_q \end{bmatrix}. \quad (9)$$

The quasi-triangle waves in zero sequence generated by both SVPWM modules can be consequently counteracted due to the phase shift. The phase shift is achieved by reconstructing the voltage references signal instead of modifying the SVPWM modules.

Since the operation frequency of the OW-PMSM varies according to conditions, the frequency of the zero circulating current will also change with it. The zero sequence current controller should be adaptive to the frequency variation. Hence, the FA-PR controller is adopted, which is shown in Fig. 13.

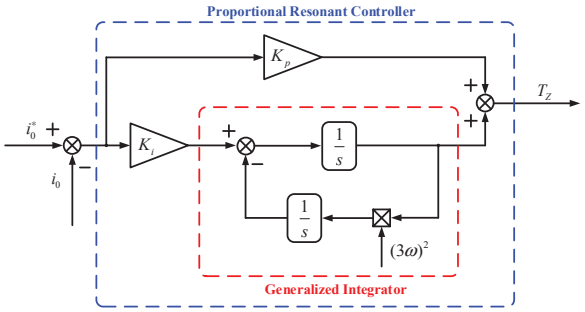

Fig. 13 Block diagram of the FA-PR controller.

The transfer function of the FA-PR is

$$C(s) = K_p + \frac{K_i s}{s^2 + (3\omega)^2} \tag{10}$$

where K_p is the proportional coefficient, K_i is the resonant coefficient and 3ω is the resonant frequency.

When compared to conventional PI controller, the integrator is replaced by the generalized integrator. The input speed feedback is used to determine the resonant frequency of the FA-PR controller. As shown in Fig. 14, the FA-PR controller has highest gain at the selected resonant frequency, viz., 3ω. Hence, the third harmonic disturbance can be responded by the FA-PR controller. The static error of PI controller for alternating signal can be avoided when the FA-PR controller is used. Meanwhile, this controller can also adapt to variable speed condition.

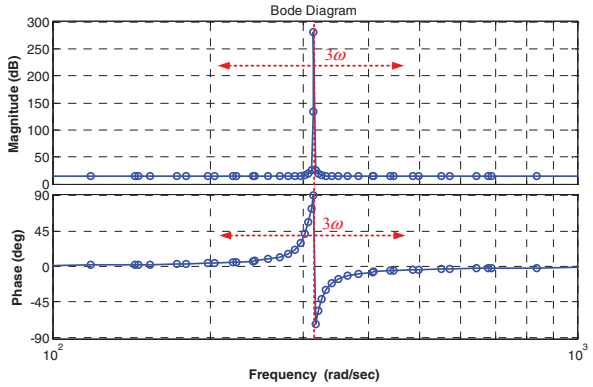

Fig. 14 Bode diagram of the FA-PR controller.

VI. Experimental Validation

The experiment platform including the 12/slot-10/pole OW-PMSM, OW connected three phase reactor and 96/slot-32/pole OW-PMSM is shown in Fig. 15. The 12/slot-10/pole OW-PMSM is used to validate the cross coupling voltages in zero sequence with zero sequence voltage measurable structure, which is shown in Fig. 16. The OW connected three phase reactor is used to verify the inverter nonlinearity effect. The suppression strategy is validated on a 3kW OW-PMSM platform based on dSPACE, which is shown in Fig. 15 (c). The switching frequency as well as the system interrupt frequency is 5kHz. The switching dead-time is set as 2μs.

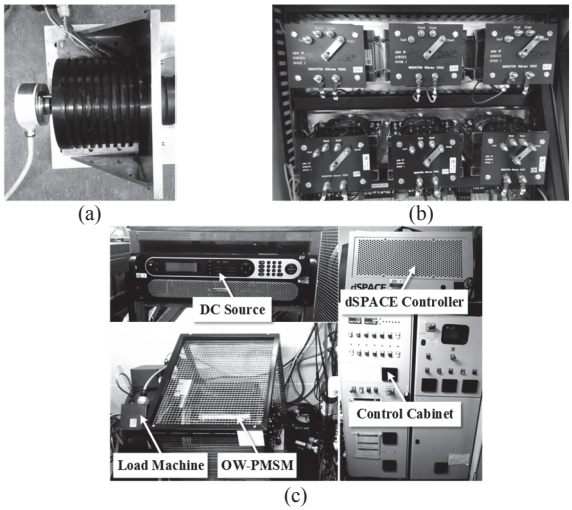

(a) (b) (c)

Fig. 15 Experiment platform pictures. (a) 12/slot-10/pole OW-PMSM. (b) OW connected three phase reactor. (c) 96/slot-32/pole OW-PMSM drives.

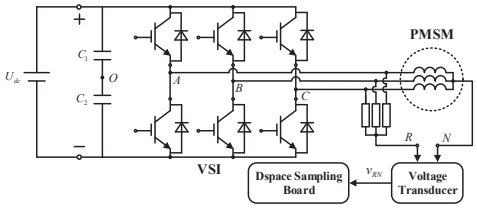

Fig. 16 System configuration of the induced zero sequence voltage measurable PMSM drive.

As for the machine side, Fig. 1 has shown the measured phase back EMF and spectrum analysis. Hence, the zero sequence back EMF has been experimentally validated. Meanwhile, Fig. 16 shows the zero sequence induced voltage measurable PMSM drive which is used to investigate the zero sequence voltage induced by armature winding currents, namely, the cross coupling voltages in zero sequence. The conventional single VSI topology has the open circuit characteristic of the equivalent zero sequence circuit. Hence, the measured voltage is just the synthesis of zero sequence back EMF and the cross coupling voltages in zero sequence from the machine side. Fig. 17 shows the measured voltage and electrical position signal at open circuit and on-load (i_q=3.62A) conditions, respectively. The distortion phenomena is in according with the analysis model and FE result which is shown in Fig. 4.

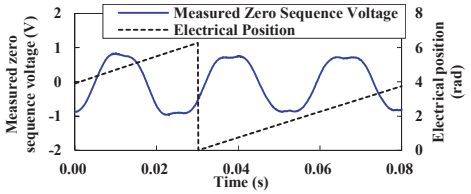

(a)

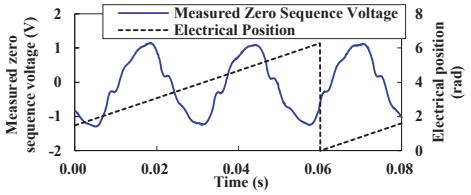

(b)

Fig. 17 Measured zero sequence voltages and electrical position signals at open circuit and on-load conditions. (a) i_q=0. (b) i_q=3.62A.

With regard to the inverter side, Fig. 18 shows the zero sequence and phase A current waveforms of the OW connected three phase reactor under small and large current conditions when 120º shift SVPWM method is applied. Before the saturation point of the reactor, the zero sequence back EMF, the modulated zero sequence voltage and the cross coupling voltages in zero sequence can be neglected. Only the inverter nonlinearity exerts an effect on the equivalent zero sequence circuit. When the phase current is in the linear region, the phase current is sinusoidal and no distinct zero sequence current emerges, which can be seen in Fig. 18 (a). However, the third harmonic zero sequence current emerges when the phase current is beyond linear region which is shown in Fig. 18 (b). The experiment results confirm the analysis model for inverter nonlinearity considering parasitic effects.

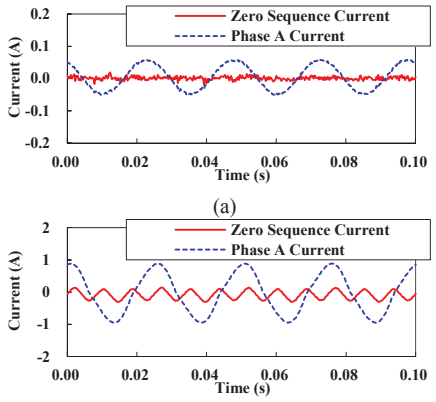

Fig. 18 Zero sequence and phase A currents of the OW connected three phase reactor under small and large current conditions. (a) Small current. (b) Large current.

Moreover, Figs. 19 and 20 show the phase currents and spectrum analysis of the OW connected three phase reactor at small current condition (eliminate the influence of inverter nonlinearity) when different shift angles are applied. Under this condition, the zero sequence back EMF, cross coupling voltages in zero sequence and inverter nonlinearity can be neglected. Hence, as confirmed by this experiment results, the 120º shift modulation method having quasi triangular zero sequence voltages fully counteracted can exhibit lowest zero sequence current.

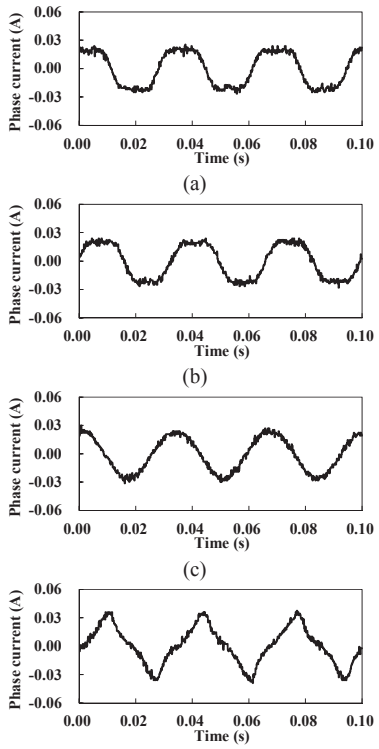

Fig. 19 Phase current waveforms of the OW connected three phase reactor with different phase shift modulation. (a) 180º shifted. (b) 150º shifted. (c) 120º shifted. (d) 90º shifted.

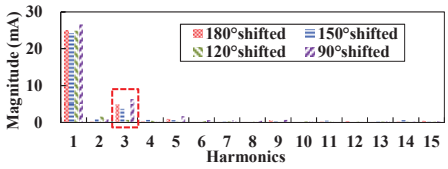

Fig. 20 Spectrum analysis of the OW connected three phase reactor with different phase shift modulation.

Finally, in order to validate the effectiveness of the suppression strategy, Fig. 21 (a) shows the phase A and zero sequence currents when controller is enabled at 5s. Figs. 21 (b) and (c) are the corresponding zoomed regions A and B in Fig. 21 (a). It can be seen that the zero sequence circulating current induced by multi sources is suppressed to zero and the relevant power losses, torque ripple and instability are consequently mitigated.

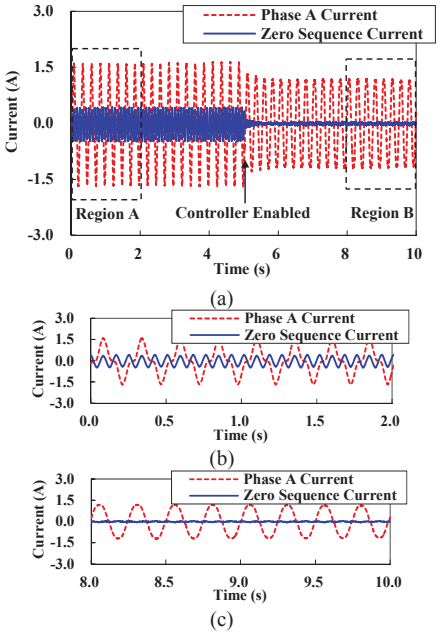

Fig. 21 Experiment results of the zero sequence circulating current suppression strategy. (a) Transient phase A and zero sequence current waveforms before and after controller enabled. (b) Before controller enabled. (c) After controller enabled.

VII. Conclusion

This paper has proposed a systematic analysis model for the zero sequence circulating current and the relevant suppression strategy of the OW-PMSM drive with common DC bus. It is found that the zero sequence back EMF, the cross coupling voltages in zero sequence, from the machine side, PWM strategy modulated zero sequence voltage and inverter nonlinearity, from the inverter side, all contribute to the formation of zero sequence voltage disturbance. The influence of the cross coupling voltages in zero sequence mainly depend on the winding configurations. The inverter nonlinearity exhibits resistive characteristic in small current condition because of the parasitic effects of the switching device, which induces almost no zero sequence disturbance voltage. But it is dominant when the phase currents are beyond the small current region. Experiment results have confirmed the analysis and the proposed suppression strategy.

APPENDIX A

TABLE I
SPECIFICATION OF TWO PROTOTYPE OW-PMSMS

Parameter	OW-PMSM I	OW-PMSMS II
Pole number	10	32
Slot number	12	96
Stack length	50 mm	110 mm
Airgap length	1 mm	2 mm
Slot opening	2 mm	5.58 mm
Stator bore radius	28.5 mm	N/A
Stator outer radius	N/A	195.2 mm
Magnet thickness	3 mm	4.5 mm
Magnet remanence	1.2 T	1.2 T
Magnet conductivity	$6.67\times10^5\ (\Omega\text{m})^{-1}$	$6.67\times10^5\ (\Omega\text{m})^{-1}$
Series turns per phase	132	832
Tooth tip width	12.92 mm	7.19 mm
Pole-pitch	17.91 mm	37.62 mm

APPENDIX B

The three phase stator inductance matrix $\mathbf{L_s}$ is

$$\mathbf{L_s}=\begin{bmatrix} L_{aa} & M_{ab} & M_{ac} \\ M_{ba} & L_{bb} & M_{bc} \\ M_{ca} & M_{cb} & L_{cc} \end{bmatrix}$$

$$=\begin{bmatrix} L_{s0}-L_{s2}\cos 2\theta & -M_{s0}-M_{s2}\cos 2(\theta+\frac{2\pi}{3}) & -M_{s0}-M_{s2}\cos 2(\theta-\frac{2\pi}{3}) \\ -M_{s0}-M_{s2}\cos 2(\theta+\frac{2\pi}{3}) & L_{s0}-L_{s2}\cos 2(\theta-\frac{2\pi}{3}) & -M_{s0}-M_{s2}\cos 2\theta \\ -M_{s0}-M_{s2}\cos 2(\theta-\frac{2\pi}{3}) & -M_{s0}-M_{s2}\cos 2\theta & L_{s0}-L_{s2}\cos 2(\theta+\frac{2\pi}{3}) \end{bmatrix}.$$

The synchronous inductance matrix $\mathbf{L_{dq0}}$ is

$$\mathbf{L_{dq0}}=\mathbf{C}^{-1}\mathbf{L_s}\mathbf{C}=\begin{bmatrix} L_d & L_{qd} & L_{0d} \\ L_{dq} & L_q & L_{0q} \\ L_{d0} & L_{q0} & L_0 \end{bmatrix}$$

$$=\begin{bmatrix} L_d & 0 & 2L_\Delta\cos 3\theta \\ 0 & L_q & -2L_\Delta\sin 3\theta \\ L_\Delta\cos 3\theta & -L_\Delta\sin 3\theta & L_0 \end{bmatrix}$$

where $\mathbf{C}$ satisfies

$$\mathbf{C}=\begin{bmatrix} \cos\theta & -\sin\theta & 1 \\ \cos(\theta-\frac{2\pi}{3}) & -\sin(\theta-\frac{2\pi}{3}) & 1 \\ \cos(\theta+\frac{2\pi}{3}) & -\sin(\theta+\frac{2\pi}{3}) & 1 \end{bmatrix}.$$

REFERENCES

[1] B. A. Welchko and J. M. Nagashima, "The influence of topology selection on the design of EV/HEV propulsion systems," *IEEE Trans. Power. Electron. Lett.,* vol. 1, no. 2, pp. 36-40, Jun. 2003.

[2] K. Mu-Shin and S. Seung-Ki, "Control of an open-winding machine in a grid-connected distributed generation system," *IEEE Trans. Ind. Appl.*, vol. 44, no. 4, pp. 1259-1267, Jul./Aug.. 2008.

[3] Y. Wang, D. Panda, T.A. Lipo and D. Pan, "Open-winding power conversion systems fed by half-controlled converters," *IEEE Trans. Power. Electron.,* vol. 28, no. 5, pp. 2427-2436, May 2013.

[4] H. Nian and Y. Zhou, "Investigation of open-winding PMSG system with the integration of fully controlled and uncontrolled converter," *IEEE Trans. Ind. Appl.*, vol. 51, no. 1, pp. 429-439, Jan./Feb. 2015.

[5] A. M. EL-Refaie, J. P. Alexander, S. Galioto, P. B. Reddy, K. Huh, P. D. Bock and X. Shen, "Advanced high-power-density interior permanent magnet motor for traction applications," *IEEE Trans. Ind. Appl.*, vol. 50, no. 5, pp. 3235-3248, Sep./Oct. 2014.

[6] Z.Q. Zhu, "Switched flux permanent magnet machines - Innovation continues" in *Proc.* ICEMS, Aug. 2011, pp. 1-10.

[7] Y. Zhou and H. Nian, "Zero-Sequence current suppression strategy of open-winding PMSG system with common DC bus based on zero vector redistribution," *IEEE Trans. Ind. Electron.*, vol. 62, no. 6, pp. 3399-3408, Jun. 2015.

[8] Q. An, J. Liu, Z. Peng, L. Sun and L. Sun, "Dual-space vector control of open-end winding permanent magnet synchronous motor drive fed by dual inverter," *IEEE Trans. Power. Electron.,* in press.

[9] A. Somani, R. K. Gupta, K. K. Mohapatra and N. Mohan, "On the causes of circulating currents in PWM drives with open-end winding AC machines," *IEEE Trans. Ind. Electron*., vol. 60, no. 9, pp. 3670-3678, Sep. 2013.

[10] V. Oleschuk, A. Sizov, B. K. Bose, and A. M. Stankovic, "Phase-shift based synchronous modulation of dual inverters for an open-end winding motor drive with elimination of zero-sequence currents," in *Proc. Int. Conf. Power Electron. Drives Syst.*, 2005, vol. 1, pp. 325-330.

[11] A. P. Sandulescu, F. Meinguet, X. Kestelyn, E. Semail and A. Bruyere, "Flux-weakening operation of open-end winding drive integrating a cost-effective high-power charger," *IET Electr. Syst. Transp.,* vol. 3, no. 1, pp. 10-21, Mar. 2013.

[12] V. T. Somasekhar, K. Gopakumar, A. Pittet, and V. T. Ranganathan, "PWM inverter switching strategy for a dual two-level inverter fed open end winding induction motor drive with a switched neutral," *Proc. Inst. Elect. Eng.*, vol. 149, no. 2, pp. 152–160, Mar. 2002.

[13] N. Bodo, M. Jones and E. Levi, "A space vector PWM with common-mode voltage elimination for open-end winding five-phase drives with a single DC supply," *IEEE Trans. Ind. Electron.*, vol. 61, no. 5, pp. 2197-2207,May 2014.

[14] J. Hwang and H. Wei, "The current harmonics elimination control strategy for six-leg three-phase permanent magnet synchronous motor drives," *IEEE Trans. Power. Electron.,* vol. 29, no. 6, pp. 3032-3040, Sep. 2014.

[15] G. Qi, J. T. Chen, Z. Q. Zhu, D. Howe, L. B. Zhou and C. L. Gu, "Influence of skew and cross-coupling on flux-weakening performance of permanent-magnet brushless AC machines," *IEEE Trans. Magn*., vol. 45, no.5, pp. 2110-2117, May 2009.

[16] L. M. Gong and Z. Q. Zhu, "Modeling and compensation of inverter nonlinearity effects in carrier signal injection-based sensorless control methods from positive sequence carrier current distortion", in *Proc. IEEE Energy Convers. Congr. Expo. (ECCE),* 2010, pp. 3434-3441.

[17] G. Wang, L. Qu, H. Zhan, J. Xu, L. Ding, G. Zhang, and D. Xu, "Self-commissioning of permanent magnet synchronous machine drives at standstill considering inverter nonlinearities," *IEEE Trans. Power Electron.,* vol. 29, no. 12, pp. 6615-6627, Dec. 2014.